Rotating Coherent Flow Structures as a Source for Narrowband Tip Clearance Noise from Axial Fan

Tao Zhu[*1], Dominic Lallier-Daniels[†2], Marlène Sanjosé[†3], Stéphane Moreau[†4] and Thomas H. Carolus[*5]
Universität Siegen, 57068 Siegen, Germany
† *Université de Sherbrooke, QC J1K2R1 Sherbrooke, Canada*

The sound radiation of axial fans typically increases significantly as the tip clearance is increased. In addition to the broadband tip clearance noise at the design flow rate, narrowband humps associated with tip clearance noise are also observed in the acoustic spectra measured in the free-field at lower flow rate. In this study, both experimental and numerical methods are used to shed more light on the noise generation mechanism of this narrowband tip clearance noise. The successful validation of the aeroacoustic predictions from unsteady simulations with the Lattice-Boltzmann Method (LBM) ensures that employing LBM data to conduct a comprehensive modal analysis for detecting rotating coherent flow structures which might be considered as noise sources. It is found that the narrowband humps are related to the tip clearance noise that is generated by an interaction of coherent flow structures being present in the tip region with the leading edge of the impeller blades. The visualization of the coherent structures is shown that they are indeed parts of the unsteady tip clearance vortex structures. They are hidden in a complex spatially and temporally inhomogeneous flow field, but can be recovered by means of appropriate filtering techniques.

Nomenclature

$\dot{V}$ = volume flow rate
Az = azimuthal position
BPF = blade passing frequency
C = chord length
c_0 = sound speed
C_{xy} = coherence
D_a = duct diameter
f = frequency
f_{int} = interaction frequency between modes and blades
f_{s-Exp} = sampling frequency
LBM = Lattice-Boltzmann Method
LCM = Least Common Multiple
LE = blade leading edge
L_{p5} = sound pressure level in free-field (anechoic room)
LRF = Local Reference Frame
M = impeller torque
m = mode order
n = impeller rotational speed
N_{int} = number of independent interactions between modes and blades
n_{mod} = mode rotational speed

N_{ppw}	=	number of points per wavelength
p_0	=	reference pressure
Pxx	=	pressure probe XX on blade pressure side
R	=	radius/radial position
R_a	=	duct radius
RI	=	rotating instability
RNG	=	Renormalization Group
s	=	tip clearance size
Sxx	=	pressure probe XX on blade suction side
S_{xy}	=	cross power spectral density
T	=	measurement/simulation time
TE	=	blade tailing edge
VLES	=	Very Large Eddy Simulation
VR	=	Voxel Refinement
z	=	number of blades
Δf	=	frequency resolution
Δp_{ts}	=	total-to-static pressure rise
Δt	=	time step
Δx	=	grid resolution in VR-zones by LBM
$\Delta \theta$	=	tangential resolution
ϑ_{xy}	=	angular spacing between two measurement points
ϕ	=	flow rate coefficient
γ_{xy}	=	phase lag
η_{ts}	=	total to static efficiency
λ	=	shaft power coefficient
ρ	=	density of air
υ	=	hub to duct ratio
ψ_{ts}	=	total to static pressure rise coefficient

I. Introduction

The aerodynamic and aeroacoustic performance of axial fans are strongly affected by the unavoidable tip clearance. Aerodynamic losses and sound radiation increase significantly as the tip clearance is increased. Several studies based on an axial fan with experimental and numerical investigations by Zhu and Carolus[1, 2] have shown that, at a healthy operating point (design point) the strong tip clearance vortices induced due to a large tip gap (s/D_a = 1.0%) interact with the fan blade surfaces, which generally produces broadboad tip clearance noise. At lower flow rate, narrowband humps associated with tip clearance noise are also observed in the acoustic spectra measured in the free-field, as shown in Figure 1. Similar issues regarding the tip clearance flow of an axial fan with a large tip gap were also investigated by Kameier and Neise[3], März[4] and more recently Pardowitz et al.[5, 6], who suggested that this kind of narrowband hump in the acoustic spectra was attributable to a so called "Rotating Instability" (RI) developing in the blade tip region. Similar observations were reported in the case of a ring-shrouded axial fan, first on the fan-alone flush-mounted on the test rig by Magne et al.[7] and Moreau and Sanjose[8], and later on the complete engine cooling module by Piellard et al.[9], and Lallier-Daniels et al.[10]. The noise mechanism was explained as the interaction between coherent structures forming in the tip region ahead of the fan and originating from the backflow from the ring gap with the fan blades.

The object of present work is to shed more light on the noise generation mechanism of this narrowband tip clearance noise, using both experimental and numerical methods. Employing unsteady simulations with Lattice-Boltzmann-Method, a comprehensive modal analysis can be done to detect rotating coherent flow structures induced from the complex and unsteady tip clearance flow, which might be considered as noise sources.
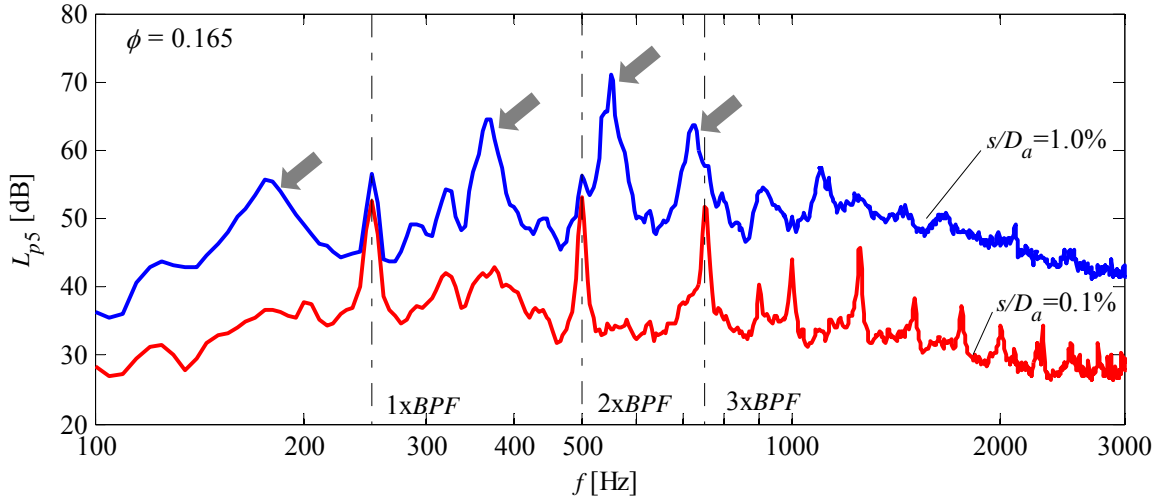
Figure 1. Far field sound pressure level measured at a part load operating point, Δf_{Exp} = 5 Hz.

II. Methodology

A. Investigated Fan

An axial fan impeller, shown in Figure 2 (left), was designed with an in-house blade element momentum based design code for low pressure axial fans (dAX-LP, see Carolus[11]). Instead of having a free vortex design, the blade loading is 70% at hub and 120% at tip, distributed approximately linearly in the spanwise direction. The additional loading of the blade tip is done intentionally to provoke strong secondary tip flow that is eventually responsible for tip clearance noise. Further design parameters are compiled in Table 1. Two impellers with different diameters were manufactured, providing a variation of tip clearance; one with a large tip clearance ratio s/D_a = 1.0% (i.e. a clearance of 3 mm) and one with an extremely small gap of s/D_a = 0.1% (i.e. a clearance of 0.3 mm). As shown in Figure 2 (right) thin supporting struts were mounted one duct diameter downstream of the rotor, so that rotor/strut interaction was minimized.
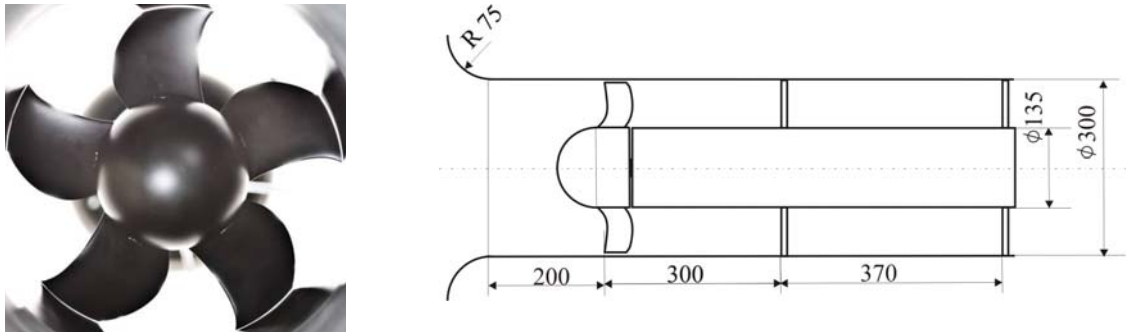

Figure 2. Manufactured impeller and fan assembly.

Table 1. Important impeller design parameters

Duct diameter	D_a	[mm]	300	Design flow rate coefficient	ϕ	[-]	0.195
Hub to duct ratio	ν	[-]	0.45	Density of air	ρ	kg/m³	1.2
Number of blades	z	[-]	5	Rotational speed	n	rev/min	3000

B. Aerodynamic and Acoustic Measurements and Data Evaluation

The aerodynamic fan performance was determined on a standard plenum test rig for fans according to the German DIN 24163 standard. Given that Δp_{ts} is the total-to-static pressure rise and M the true rotor torque applied, the following non-dimensional fan performance coefficients are used:

flow rate coefficient

$$\phi = \frac{\dot{V}}{\frac{\pi^2}{4}D_a^{\,3}\cdot n} \tag{1}$$

total to static pressure rise coefficient

$$\psi_{ts} = \frac{\Delta p_{ts}}{\frac{\pi^2}{2}\rho D_a^2 n^2} \tag{2}$$

shaft power coefficient

$$\lambda = \frac{2\pi nM}{\frac{\pi^4}{8}\rho D_a^5 n^3} \tag{3}$$

and total to static efficiency

$$\eta_{ts} = \frac{\dot{V}\Delta p_{ts}}{2\pi nM} \tag{4}$$

The aeroacoustic investigations were carried out on a standardized acoustic duct test rig for fans with a semi-anechoic room (4.50 m×3.50 m×3.23 m) according to DIN ISO 5136 standard, as shown in Figure 3. The impeller takes the air from a large semi-anechoic room and exhausts into a duct with an anechoic termination. The flow rate is controlled by a throttling plate downstream of the termination and is determined by a calibrated hot-film probe in the duct.
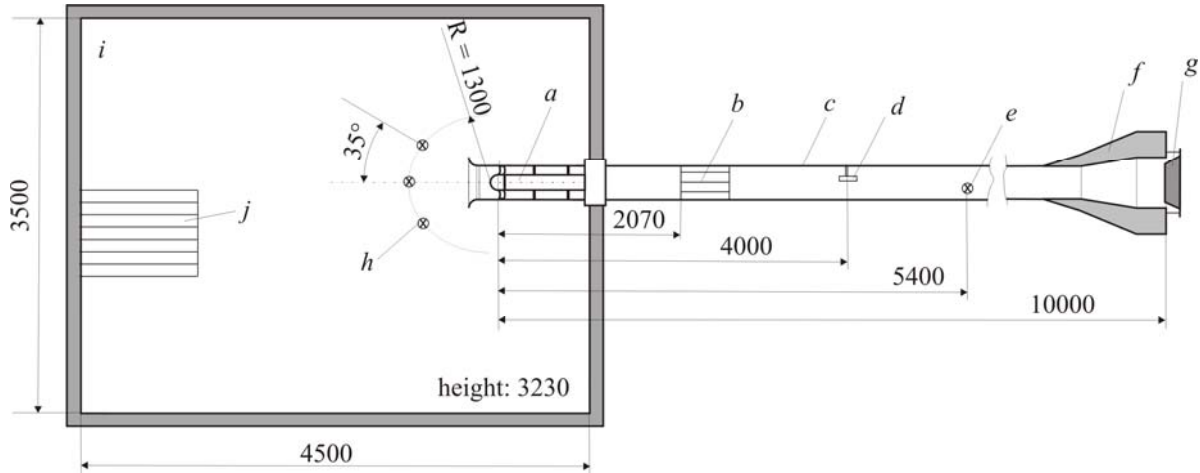

Figure 3. Duct test rig with semi-anechoic chamber (top view); (a) fan assembly (center line 1350 mm above reflecting ground), (b) star flow straightener, (c) duct, (d) in-duct microphone, (e) hot-film mass-flow meter, (f) anechoic termination, (g) adjustable throttle, (h) free-field microphones, (i) semi-anechoic chamber, (j) air-inlet grid on ground.

The suction side sound pressure level L_{p5} (averaged through three microphones) is measured in the free-field of the anechoic room by three microphones (Brüel & Kjaer, type 4190), placed on a virtual hemispherical measurement surface around the inlet. All time signals were captured with a sampling frequency $f_{s\text{-}Exp} = 25.6$ kHz. The spectral analysis is based on the power spectral density (PSD) which was obtained by the function *pwelch* in MATLAB[®] Vers. R2012a. The parameters chosen for *pwelch* were *window = hann(nfft)*, *noverlap = 0*, *nfft = fs·T/n$_{ave}$* (*n$_{ave}$*:

number of averages). To make a fair comparison with the results from LBM, which has only relative short time signals, the *nfft* length to obtain a frequency resolution of $\Delta f_{Exp} = fs/nfft = n_{ave}/T = 5$ Hz (with $n_{ave} = 50$, $T = 10$ s) in all spectra is chosen. For all levels, the reference pressure is $p_0 = 2\cdot10^{-5}$ Pa. All overall levels are the sum of narrow band levels from 100 Hz to 3 kHz (limited by the f_{max} in LBM-results, see Equation 5).

C. Measurement of Surface Pressure Fluctuation

In addition to the acoustic measurements, two adjacent blades of each impeller were instrumented with eight flush mounted miniature pressure transducers (Knowles Acoustics type *FG-3329-P07*) to measure wall-pressure fluctuations. The transducers employed are basically miniature condenser microphones with a sensitive diameter of 0.7 mm and protection grid on top. The protection grid was flush-mounted with the blade surface. One set was placed on the blade suction surface (denoted *Sxx*) of one blade while the other series was located on the pressure side (*Pxx*) of the second blade. Note that all instrumented transducers were located in the same blade passage, as shown in Figure 4. It was verified that the instrumentation of the transducers had no effect on the aerodynamic and acoustic performance (see Zhu[12]). A slip-ring transducer transfers the signals from the rotating to the stationary laboratory system. The random noise from the slip-ring transducer was found to be negligible. The signals from the transducers in the tip region (*S01* to *S13* and *P01* to *P11*) as well as the three free-field and the in-duct microphones were recorded synchronously to allow a correlation analysis.

All the miniature pressure transducers were calibrated in-situ with a white noise excitation signal ranging from 100 Hz to 10 kHz, as shown in Figure 4. The spectral analysis method of the acquired time signals from the miniature pressure transducers is identical as the one described in the previous section.
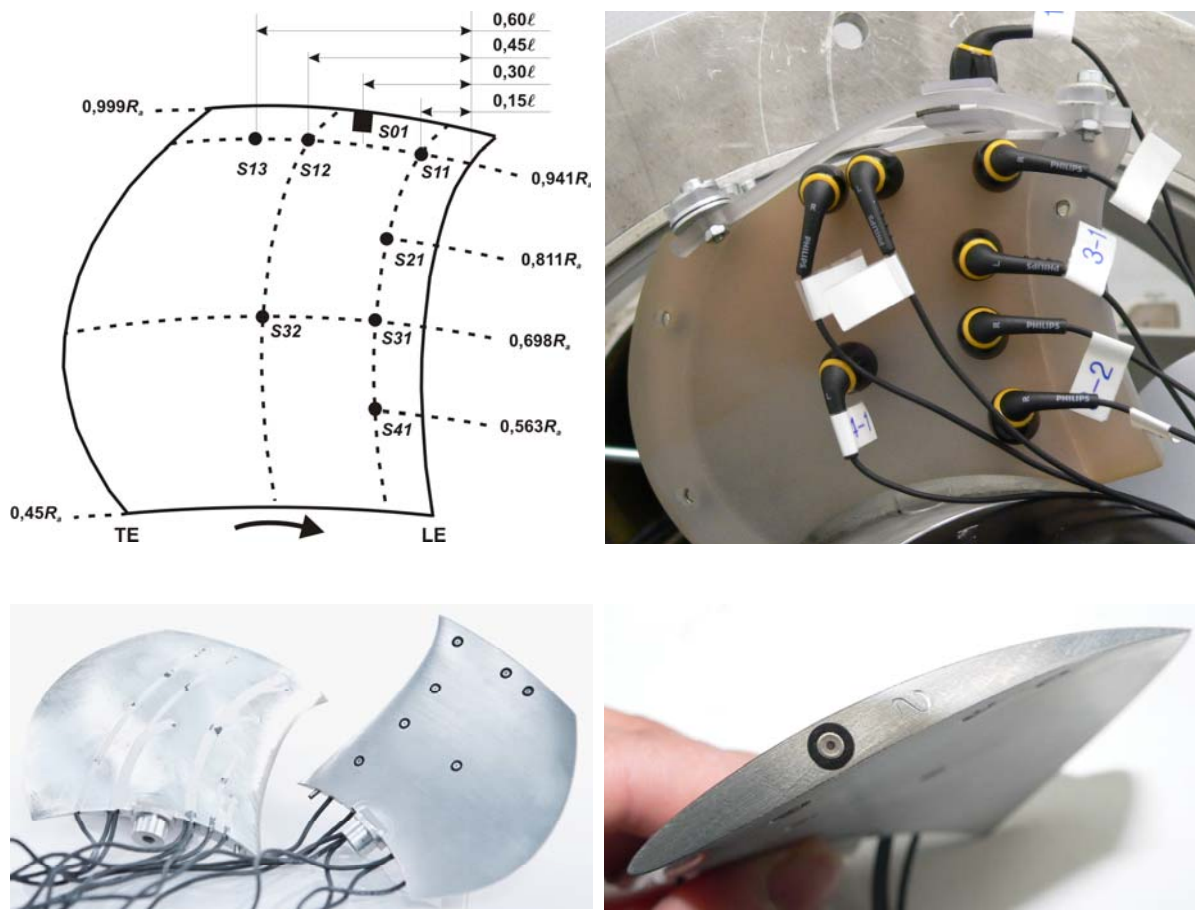

Figure 4. Position of the miniature pressure transducer on blade suction surface (upper left), the instrumented blade (lower row) and arrangement for the calibration (upper right).

D. Lattice-Boltzmann Method

To predict the unsteady flow phenomena associated with the tip flow and the generation and radiation of sound, a Lattice-Boltzmann Method (LBM) is used. LBM-based methods are by nature explicit, transient and compressible. Unlike conventional CFD methods based on discretizing the macroscopic continuum equations, LBM starts from "mesoscopic" kinetic equations, i.e. the Boltzmann equation, to predict macroscopic fluid dynamics[13, 14]. The basic idea of LBM is to track the advection and collisions of fluid particles. Since the average number of particles in a representative volume of fluid far exceeds the available computing power required to track them individually, the particles are grouped into a set of discrete *i*-directions. The computation follows the particle distribution function f_i which represents the number of particles in a unit of volume at a specific time and location moving with velocity c_i. As in statistical physics, the flow variables such as density and velocity are determined by taking the appropriate moments, i.e. summations over the set of discrete directions, of the particle distribution function.

In this study the commercial code PowerFlow™ version 5.0c is used. In order to model the effects of unresolved small scale turbulent fluctuations, in this code the Lattice-Boltzmann equation is extended by replacing its molecular relaxation time scale with an effective turbulent relaxation time scale derived from a systematic Renormalization Group (RNG) procedure (see details in Chen et al[15-17]). A turbulent wall-model, including the effect of pressure gradients, is also integrated into the solver. This method is called Very Large Eddy Simulation (VLES) and has been validated and used for several aeroacoustic problems[9, 18-21]. The LBM scheme is solved on a grid composed of cubic volumetric elements, also called voxels, using a Voxel Refinement (VR) strategy, where the grid size changes by a factor of two for adjacent resolution regions. For the simulations of flows in domains consisting of rotating and stationary regions, the computational domain is divided into a so called "body-fixed" Local Reference Frame (LRF) and a "ground-fixed" reference frame domain, connected by an interface (see details in Zhang et al.[22]).

E. Numerical Setup

In the simulation, the computational domain is representative of the complete full scale acoustic test rig shown in Figure 3. For simplicity all inner walls of the semi-anechoic room (i.e. even the floor) are defined as porous media that serves to absorb acoustic waves and prevent their reflection back to the source. The air inlet and outlet regions also include damping zones to avoid acoustic reflections. All other surfaces (nozzle, duct, fan impeller and fan hub) are specified as perfectly rigid walls. The mass flow according to the required fan operating point is specified at the inlet. Free exhaust at ambient atmospheric pressure is assumed at the outlet. The simulation is performed at the fan design point and at a part load operating point, i.e. flow rate coefficient of $\phi = 0.195$ and $\phi = 0.165$ respectively. A LRF-domain around the rotating fan impeller is discretized using the finest grid resolution of $\Delta x = 0.5$ mm (VR10) corresponding to 600 voxels across the duct diameter. The large tip clearance is resolved with 6 voxels. It is shown that the aero-acoustic effect of large tip clearance can still be captured even with this relative coarse resolution. The small tip clearance is replaced by $s/D_a = 0.0\%$, i.e. the tip clearance is completely neglected. Comparison of LBM predicted results to the experiment shows that this is an acceptable simplification. The VR-zones are denoted in Figure 5. The regions around the "microphone probes" are resolved spatially with $\Delta x_{mic} = 8.0$ mm (VR6). Assuming that the required number of points per wavelength to accurately capture acoustic waves is $N_{ppw} = 16$ (Brès, G.A. et al.[23]), the maximum frequency f_{max} that this grid can resolve should be at least

$$f_{max} \sim \frac{c_0}{N_{ppw}\Delta x_{mic}} \sim 3 \text{ kHz} \tag{5}$$

For the configurations with $s/D_a = 0.0\%$ at both operating points and with $s/D_a = 1.0\%$ at $\phi = 0.165$, the LBM-results are evaluated using the data captured over an overall time interval $T_{sim} \approx 1$ s corresponding to approx. 50 impeller revolutions upon arriving at a statistically stable fan operating point, i.e. with settled flow rate and pressure rise. The simulation time step is $\Delta t = 8.2 \cdot 10^{-7}$ s in VR10. The data at the monitoring points in the acoustic far field, i.e. at the microphone probe positions, are captured with a sampling frequency $f_{s-Probe.} = 75822$ Hz, the hydrostatic pressure fluctuations on the blade surface and in an adjacent annular volume with $f_{s-SurVol.} = 9478$ Hz. All spectra are evaluated from the raw LBM data using the same method described in last section with appropriate window length *nfft* resulting in the same frequency resolution of $\Delta f_{LBM} = 5$ Hz.
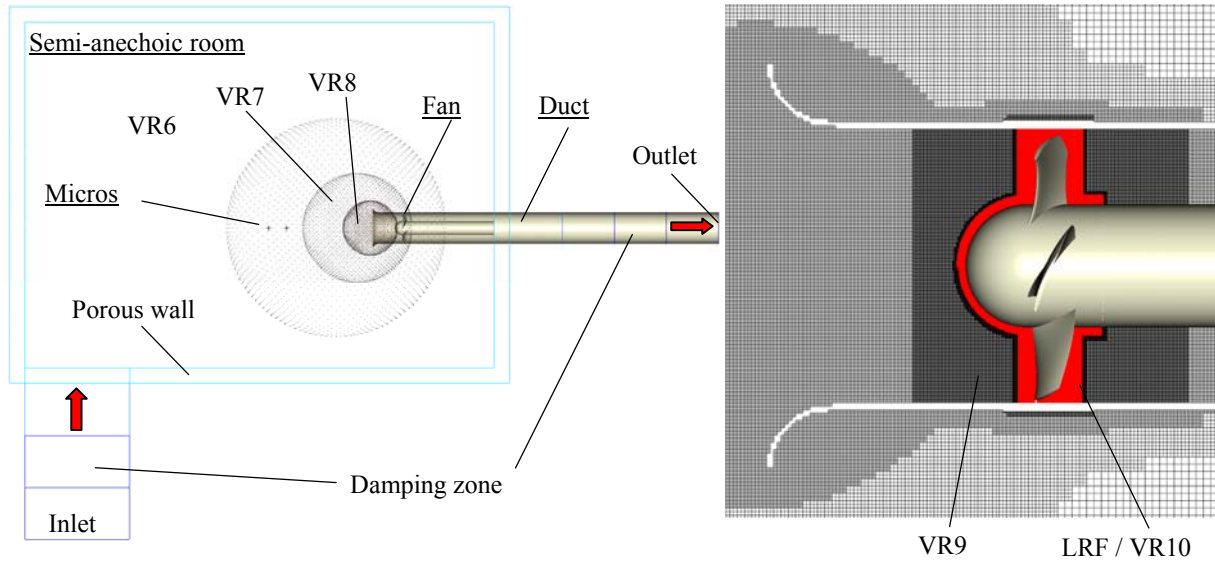
Figure 5. Simulation domain including the semi-anechoic room and test-rig duct (left), mesh details in the fan section with LRF-domain (right, red).

The fan overall pressure rise is evaluated in planes approximatively one duct diameter up- and downstream from the fan impeller, area-averaged in each plane and time-averaged during ten revolutions. It was shown in the preliminary study (Zhu and Carolus[2]) to suffice as a proper approach to yield the converged aerodynamic performances.

The configuration with $s/D_a = 1.0\%$ at $\phi = 0.165$ is simulated for a long physical time of $T_{sim} \approx 5$ s to get sufficient time resolution for performing the correlation analysis. The pressure probes on the blade surfaces are set at the exact same positions as in the experiment, as shown in Figure 6. In order to detect the rotating coherent flow structures, a number of probes are placed in the blade passages around the full 360° of the fan circumference, spanning from very close to the blade tip ($R = 146$ mm) down to the middle of the blade ($R = 110$ mm); the resulting tangential resolution is $\Delta\theta = 12°$. In the chordwise direction a series of 10 probes are uniformly distributed from the leading edge ($C01$) to the trailing edge ($C10$) along the profile chord at the blade tip. An overview of the probe setup in the LBM simulation is given in Table 2.

Table 2. Distribution of the probes in the blade passage

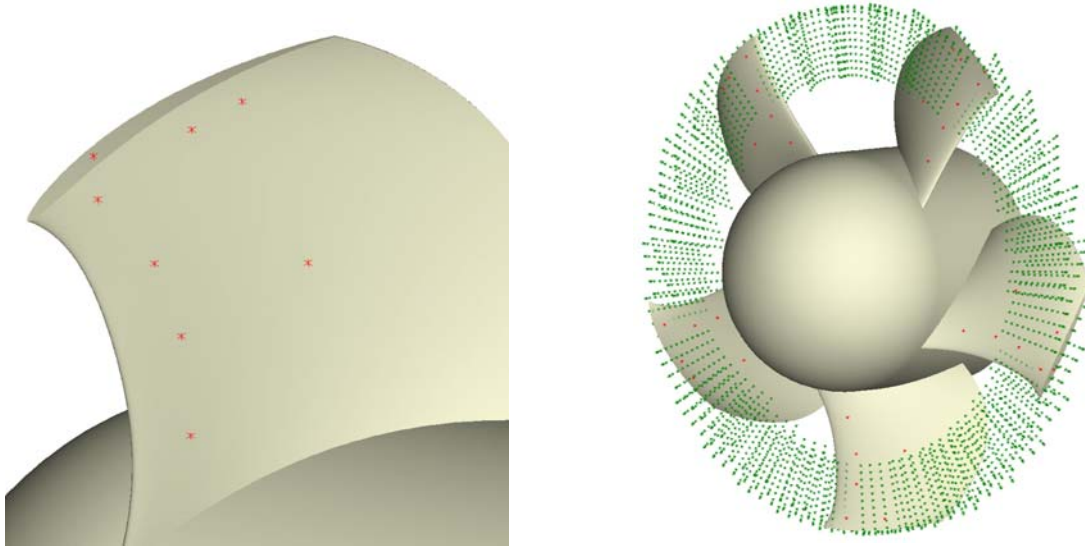| Direction	Start-Pos. (Notation)	End-Pos. (Notation)	Distribution
Spanwise (Radial)	$R = 146$ mm ($R146$)	$R = 110$ mm ($R110$)	$\Delta R = 4$ mm
Chordwise	Leading Edge (LE) ($C01$)	Trailing Edge (TE) ($C10$)	10 probes uniformly distributed from LE to TE along the profile chord at blade tip
Azimuthal	5 rows of probes ($C01$-$C10$) in each blade passage, around full 360° (5 blade passages) ($Az01$)	($Az25$)	$\Delta\theta = 12°$ (in each blade passage)

Figure 6. Setup of the probes in LBM: probes on the blade surfaces (left) and an overview of the probes in the blade passage (right).

F. Modal Analysis for Detecting Rotating Coherent Flow Structures

Working under the assumption that coherent structures generated from the tip gap flow and their interaction with the blades are responsible for the narrowband humps observed in the acoustic spectra in Figure 1, the difficulty thus becomes to properly identify those structures and model their interaction with the blades.

To accomplish this, a coherent structure analysis method previously used on centrifugal[24-28] and axial fans[29] was considered as a basis. The method hypothesizes that structures identified with it can be viewed as circumferential wave patterns superimposed on the base flow, rotating at a certain velocity potentially very different from the base rotor speed.

These flow patterns, through their interaction with the fan blades, would cause periodic fluctuations in blade loading and thus produce tones in the free-field; adding the contribution of the different modes together would generate the observed narrowband humps in the spectra. These wave patterns can be quantified through two parameters: their mode order m and rotational speed of the mode n_{mod}. From these characteristics, their interaction frequency with the rotor blades can be calculated. It should be noted that the term mode as used in this work refers to the coherent flow structures detected using the current modal analysis method in the aerodynamic near field around the fan impeller; it should not be mixed up with the term mode which is also used to define acoustic modes propagating in a duct.

To calculate the properties of the wave patterns, the modal method relies on the use of synchronous measurements of flow properties at two or more points along the circumference at a given radial position. Using time signals of two sequential measurement positions, the cross power spectral density (CPSD) S_{xy} can be computed as well as the coherence C_{xy} between the two signals. In the course of the work presented here, the CPSD is evaluated using Welch's modified periodogram method[30] implemented in MATLAB® *cpsd* function. Furthermore, the phase lag γ_{xy} between the two signals can be calculated as

$$\gamma_{xy}(f) = arctan \frac{Im\{S_{xy}\}}{Re\{S_{xy}\}} \tag{6}$$

The angular spacing between two measurement points, ϑ_{xy} being known, the method proposes the estimation of the mode order of the flow structures as

$$m(f) = \frac{\gamma_{xy}}{\vartheta_{xy}} \tag{7}$$

The maximum mode order that can be detected depends on the number of probes around the circumference. Note here that the coherence function is used as a filter to evaluate the phase only for the frequencies for which the

coherence is high. The resulting phase signal must also be beforehand corrected for multiples of 2π radians (unwrapped phase). The rotational speed of the mode in the absolute frame of reference can be calculated using stationary measurement points as

$$n_{mod} = \frac{2\pi f}{m} \tag{8}$$

and in the case of the probes rotating with the fan impeller, as

$$n_{mod} = n - \frac{2\pi f}{m} \tag{9}$$

where n is the rotational speed of the fan impeller. Thus, the identified coherent flow structures are described as a function of their frequency of occurrence with a mode order m and a rotational speed n_{mod}.

Using the mode characteristics and knowing the number of blades in the fan impeller design, the interaction frequency f_{int} between the rotor and the identified modes can then be calculated using the following equation:

$$f_{int} = N_{int}\left(m, z\right) \cdot \left(n - n_{mod}\right) = N_{int}\left(m, z\right) \cdot n \cdot \left(1 - \frac{n_{mod}}{n}\right) \tag{10}$$

where $N_{int}\left(m,z\right)$ represents the number of independent interactions between a given mode m and the z blades per relative rotation and is determined as the least common multiple (LCM) of m and z. This factor takes into account the fact that the interaction of a mode with a number of lobes that is a multiple of the number of fan blades (or inversely) will produce a tone at an order multiple of the modified $(1-n_{mod}/n)\cdot BPF$ fundamental, with several blades contributing at the same time, whereby the blade passing frequency (BPF) is defined as $BPF = n\cdot z$.

The original method developed at Penn State University[24-27] as revisited by Wolfram and Carolus[28] and Sturm et al.[29], however, does not specifically address the fact that a negative phase would indicate the presence of a mode rotating in a direction opposite to the direction of evaluation. In that case, the mode order will be negative and have an associated negative velocity. These modes should not be discarded as they could have a physical explanation.

Furthermore, while the method allows for the detection and identification of coherent structures as well as their possible interaction frequency from an acoustic standpoint, it only provides an "event counter" approach to the identification i.e. it does not provide any information on the amplitude of the interaction for a given event. This was also noted previously by Wolfram and Carolus[28], a qualitative comparison between the actual acoustics and structure interaction frequency histograms were later presented by Sturm et al.[29].

III.   Results

A. Validation of LBM-Predicted Aerodynamic and Acoustic Results
Aerodynamic and acoustic overall characteristics
The aerodynamic overall performance characteristics in terms of ψ_{ts}, λ and η_{ts} as a function of ϕ are shown in Figure 7 (left). The effect of the tip clearance on the aerodynamic characteristics is rather obvious: pressure rise and efficiency drop and the onset of stall moves to higher flow rates as the tip clearance is increased. The LBM-predictions at both design point and part load operation point are rather satisfactory. The acoustic performance characteristics in terms of overall sound pressure level L_{p5} (100 to 3000 Hz) in the free-field as a function of ϕ are shown in Figure 7 (right). The sound pressure as predicted from LBM reflects the effect of the tip clearance quite well: LBM and experiments show about 10 dB increase at design point ($\phi = 0.195$) and 15 dB at part load operating point ($\phi = 0.165$) due to the large clearance.
Sound pressure level spectra in free-field
The sound pressure level spectra in free-field are depicted in Figure 8, when the impellers are operated at the low flow rate $\phi = 0.165$. Both, measurements and LBM-prediction, show that the broadband sound is enhanced by increasing the tip clearance. Looking at the broadband components the agreement between experimentally determined and LBM predicted spectra is satisfactory. The peaks at the blade passing frequency (BPF) and its harmonics in the experimental results are very distinctly above the broadband level for the small tip clearance. This is not captured by the LBM simulation. However, according to a recent investigation of the same fan/test rig assembly by Sturm et al.[31], sound at the BPF and its harmonics from this isolated axial fan is related to large scale inflow distortions caused by the slow flow in the room the fan takes its air from, which can be firstly developed after a long simulation time (over 100 s physical time). The results shown in this study are all captured from simulation

after achieving a statistically stable operating point, but not sufficient for developing the large scale inflow distortion.

In the case of the large tip clearance, the narrowband humps are generally well predicted from LBM. In the experimental results the center frequencies of the narrowband humps are at approximately 185, 370, 555 and 730 Hz, which corresponds to the frequencies at $0.74 \times 1 \times BPF$, $0.74 \times 2 \times BPF$, $0.74 \times 3 \times BPF$ and $0.74 \times 4 \times BPF$ respectively. In the LBM predicted spectrum, the first three humps can be observed and the center frequencies of which are slightly shifted to 175, 350, and 525 Hz, which corresponds to the frequencies at $0.70 \times 1 \times BPF$, $0.70 \times 2 \times BPF$, and $0.70 \times 3 \times BPF$ respectively.
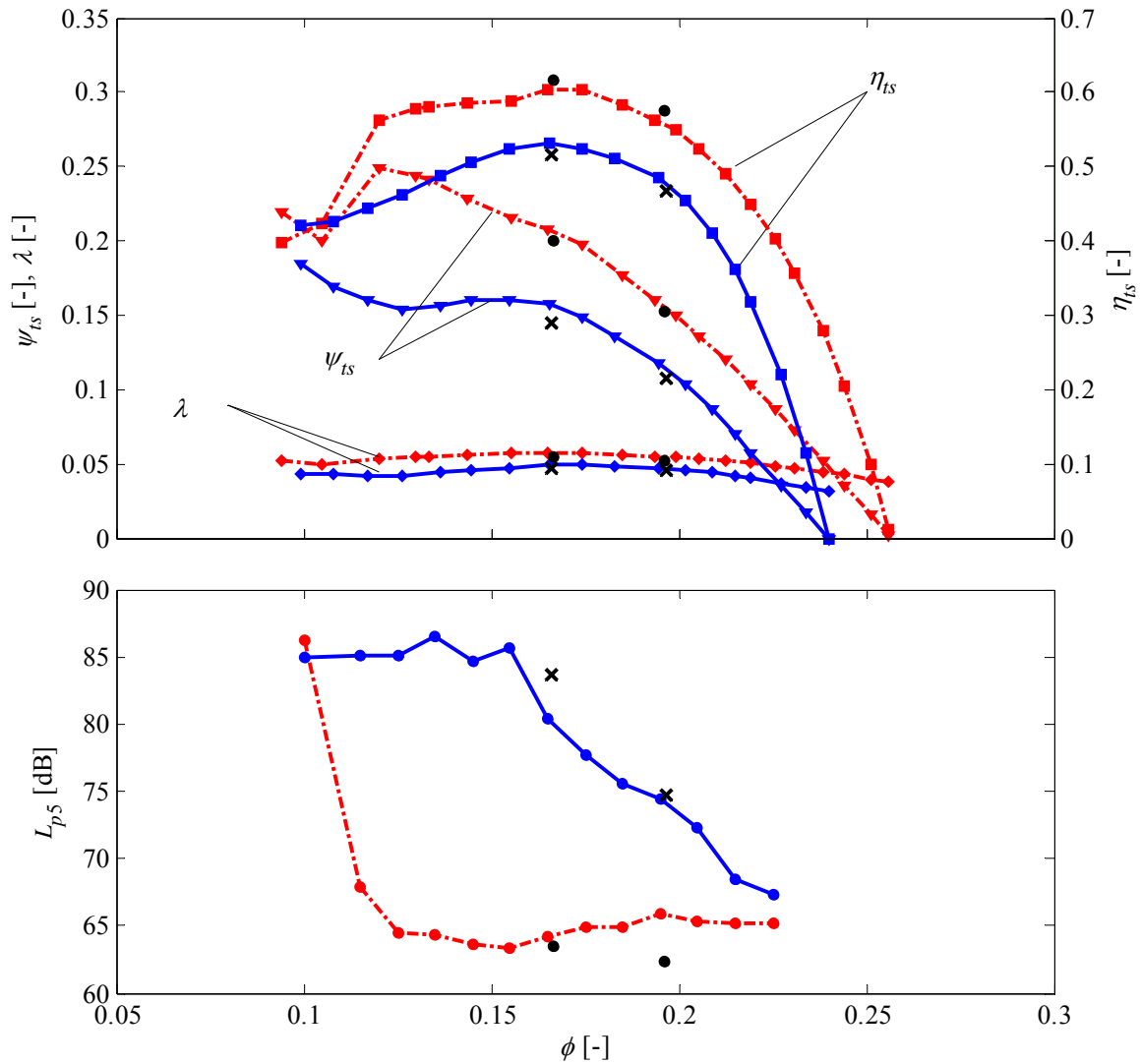

Figure 7. Aerodynamic characteristic (left) and acoustic (right) characteristics. Red (Blue): Experiment - s/D_a = 0.1% (1.0%); Black dot (cross): LBM - s/D_a = 0.0% (1.0%).
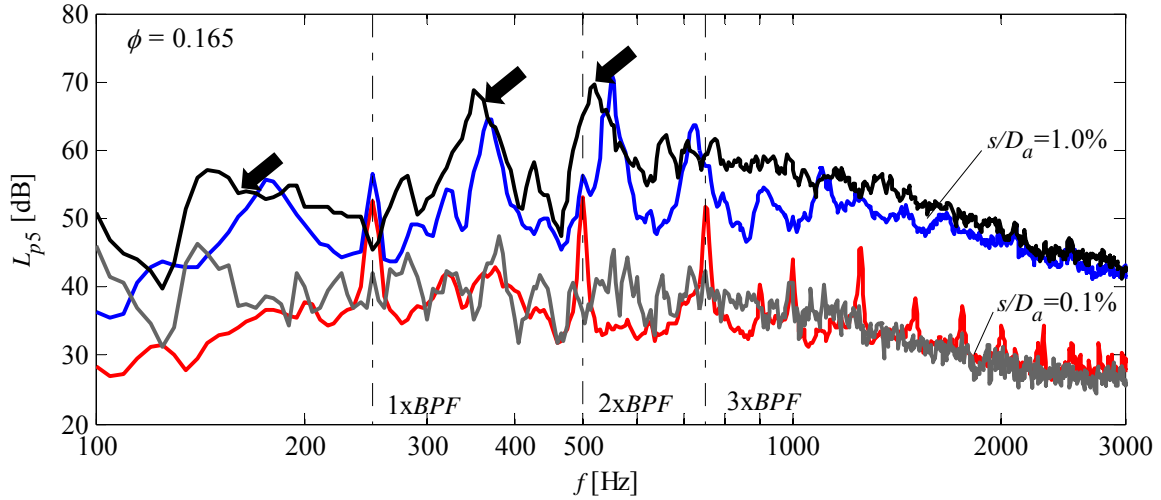
Figure 8. Sound pressure levels at low flow rate, $\Delta f_{Exp} = \Delta f_{LBM} = 5$ Hz. Red (Blue): Experiment - $s/D_a = 0.1\%$ (1.0%); Grey (Black): LBM - $s/D_a = 0.0\%$ (1.0%).

Wall-pressure on the fan blades

Another point of comparison between the LBM simulations and experiment consisted of wall-pressure measurements as recorded using the flush mounted sensors on the rotor blades (see section II.C).

The analysis of the surface pressure from a pair of probes on the blade surface: $S11$ on the suction side and $P11$ on the pressure side, located near the leading edge at the tip of the blade (see Figure 4) leads to some insight into the possible noise mechanism associated with the tip gap flow. The data captured from the experiments and LBM simulations are shown in Figure 9, in terms of wall-pressure level at each probe (top), the coherence between $S11$/$P11$ (middle) and the unwrapped phase (bottom). Both experimental and LBM results show, in a certain frequency range, high coherence levels and linear phase behavior, which indicates coherent flow structures captured traveling from one blade suction side to the pressure side of the next in one blade passage. Although there is a certain deviation between the experiment and LBM results in terms of the pressure level and the frequency range with high coherence levels, the frequency interval between the side by side peaks from both shows a value of approximately 35 Hz, which, according to the theory introduced by Kameier and Neise[3] is indicative of the so called "Rotating Instability", which rotates at about 70% of the impeller rotational speed (35 Hz/50 Hz) in the opposite direction of the impeller observed in the rotational frame, or 30% of the impeller rotational speed in the same rotating direction as the impeller observed in the stationary frame. The interaction of this so-called "Rotating Instability" with the impeller blades might be the source of the narrowband humps observed in the sound pressure level spectrum in free-field.

Yet, to our knowledge, the physical interpretation of the so-called "Rotating Instability" is still missing and not fully understood. As recently pointed out by Magne et al.[7] and Moreau and Sanjose[8], it might be interpreted as rotating coherent flow structures formed from the tip clearance vortices that interact with the blades and trigger a circumferential pressure mode or a superposition of several circumferential pressure modes, which can be only detected through the modal analysis method introduced in section II.F.

To provide such an evidence the experimental pressure fluctuations measured with the probes on the blade surfaces could be used. However, the angular spacing of the probe pairs on the blade surface, θ_{xy}, is always limited by accessibility and probe size. It is then relatively large, i.e. $\theta_{xy} = 72°$. Consequently the mode orders that can be detected unambiguously are limited, i.e. theoretically only up to $m = 360°/\theta_{xy} = 5$. Conversely, a virtually unlimited spatial resolution can be obtained by applying the correlation analysis to data from the high resolution unsteady flow field obtained by the LBM simulation. As presented in Figure 8 the narrowband humps are predicted quite well with LBM, and even the humps in the pressure fluctuations are captured on the rotating blade surfaces as shown in Figure 9. This encourages the author to apply the modal analysis to the LBM-data, which can detect the higher mode orders in a more extensive spatial range.
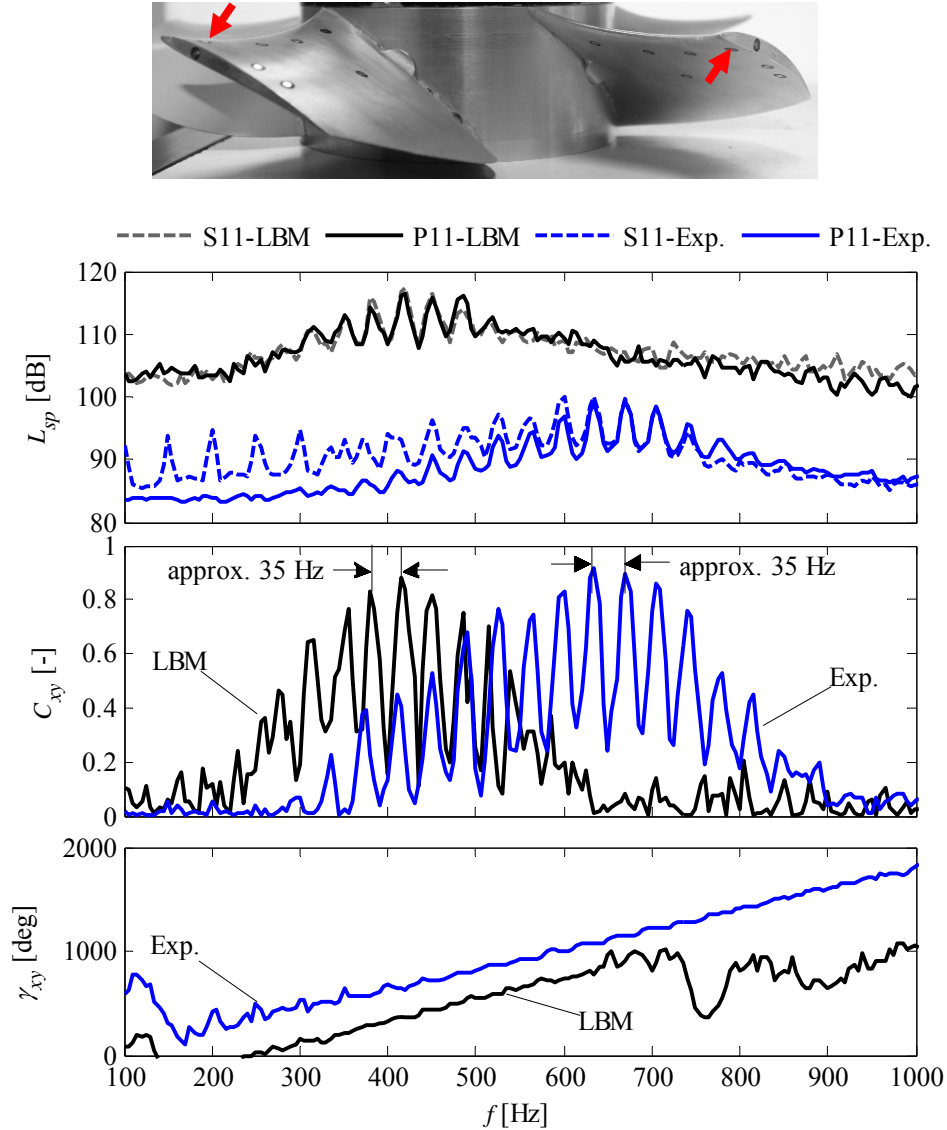
Figure 9. Surface pressure level (top), coherence (middle) and phase from probe S11 and P11 on the blade surface, comparison between Exp. and LBM, $\Delta f_{Exp} = \Delta f_{LBM} = 5$ Hz.

B. Detecting Rotating Coherent Flow Structures based on LBM data

In order to apply the proposed modal analysis method, pressure fluctuations captured from the fluid probes in the blade passages from the LBM simulation (Figure 6) are employed. This makes the unambiguously detection of mode order up to $m = 30$ with $\theta_{xy} = 12°$. Note that the fluid pressure fluctuations are collected in the rotational frame, with the fluid probes moving with the blades.

Results from a single probe pair

First of all, in order to demonstrate the modal analysis method, an example is carried out with one single probe pair at a radius of 138 mm (R138) at the leading edge (C01) is shown here. The coherence is computed for frequencies ranging from 100 to 600 Hz. This is done with prior knowledge about the coherent structures already captured with the probes on the blade surfaces (Figure 9). Using a threshold value of $C_{xy} \geq 0.6$ to identify coherent events, the chosen events show a very good linear trend when looking at the phase, as shown in Figure 10. The respective mode order m and the rotational speed of the modes n_{mod} (observed in stationary frame) can be calculated,

(Figure 11). It is found that the detected mode orders spread from $m = 3$ to $m = 18$ with a certain distribution. The linear regression of the rotational speed of the modes shows that the modes gather around approximately 30% of the rotational speed of the impeller ($n_{mod}/n = 0.3$), which corresponds to the coherence analysis from the surface pressure on the blades, although variations in a certain range can be also observed.
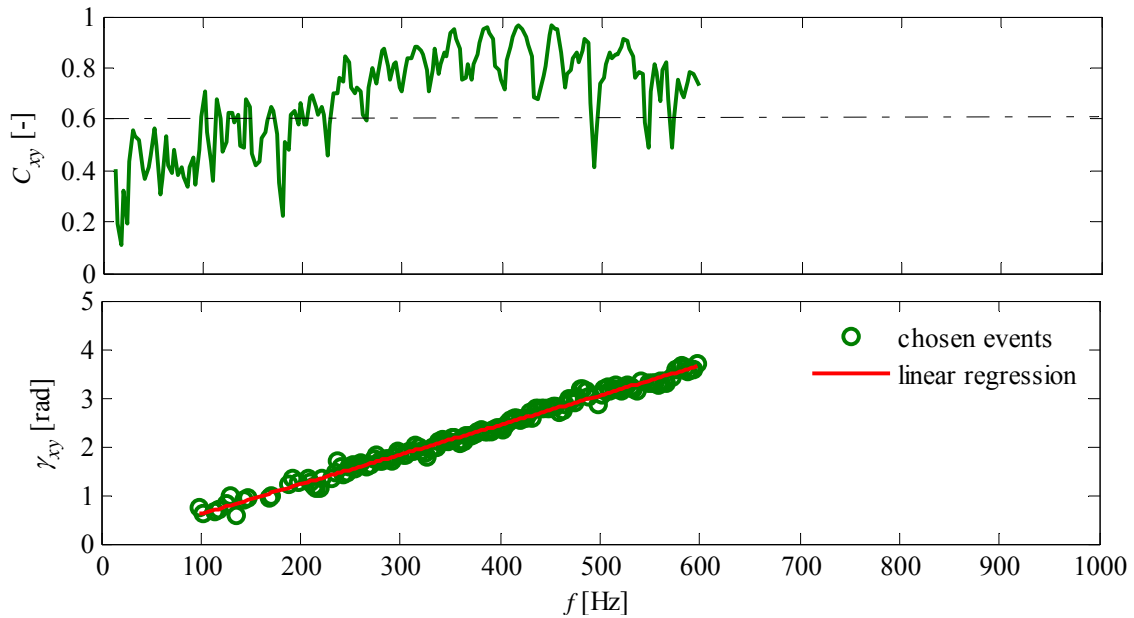

Figure 10. Coherence (top) and phase (bottom) e.g. from probe pair *R*138-*C*01-*Az*04 and -*Az*05 in LBM, presented in the frequency range 10 - 600 Hz.
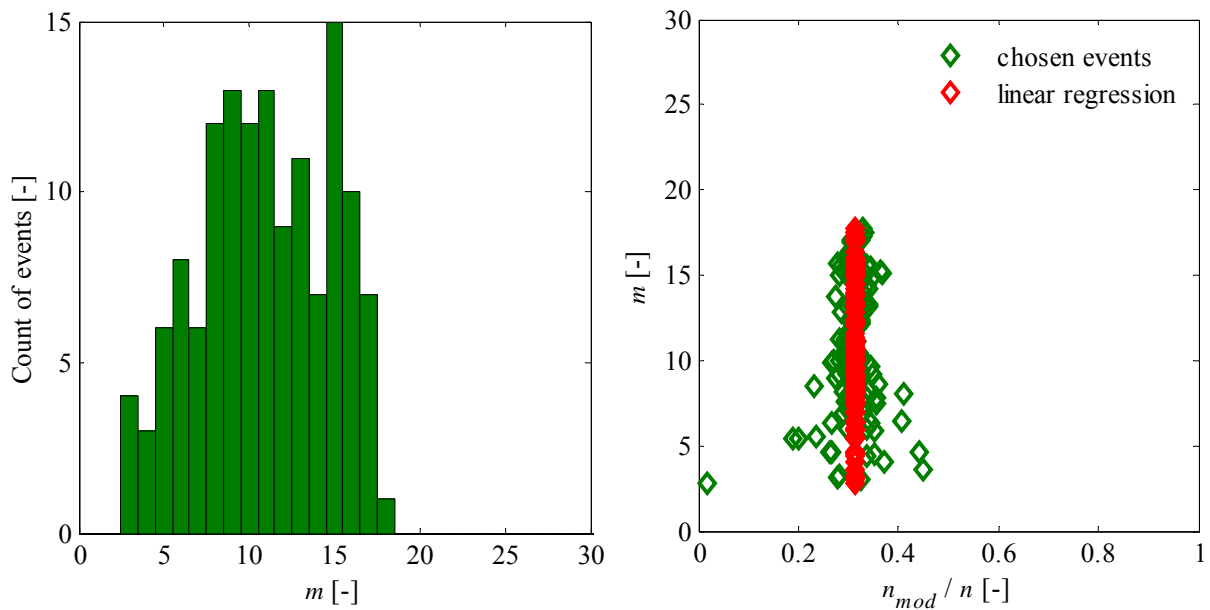

Figure 11. The mode order (left) and corresponding rotational speed (right) of the detected coherent flow structures, e.g. from probe pair *R*138-*C*01-*Az*04 and -*Az*05 in LBM.

American Institute of Aeronautics and Astronautics

Finally the interaction frequency from the detected rotating coherent flow structures and the impeller blades can be calculated (Figure 12). The interaction frequencies indicated by the highest number of events correspond quite well with the narrowband humps in the sound pressure spectrum predicted in the free-field by the LBM. Note that, as the interaction number N_{int} (m,z) defined in Equation 10 is obtained by the LCM of mode order m and blade number z, only the mode orders $m < 5$ as well as $m = 5$, 10, and 15 (multiples of the blade number z) contribute to the interaction frequency f_{int} at the center frequencies of the three narrowband humps at $0.70 \times 1 \times BPF$, $0.70 \times 2 \times BPF$, and $0.70 \times 3 \times BPF$ respectively, whereby the other mode orders yield the higher interaction frequencies. The rotational speed of the detected modes spreads in a small range, which triggers the hump form of the interaction frequencies and not a single peak. Such a statistical distribution of the rotational speed was also evidenced by Piellard et al.[9], and Lallier-Daniels et al.[10] in more complex modules.
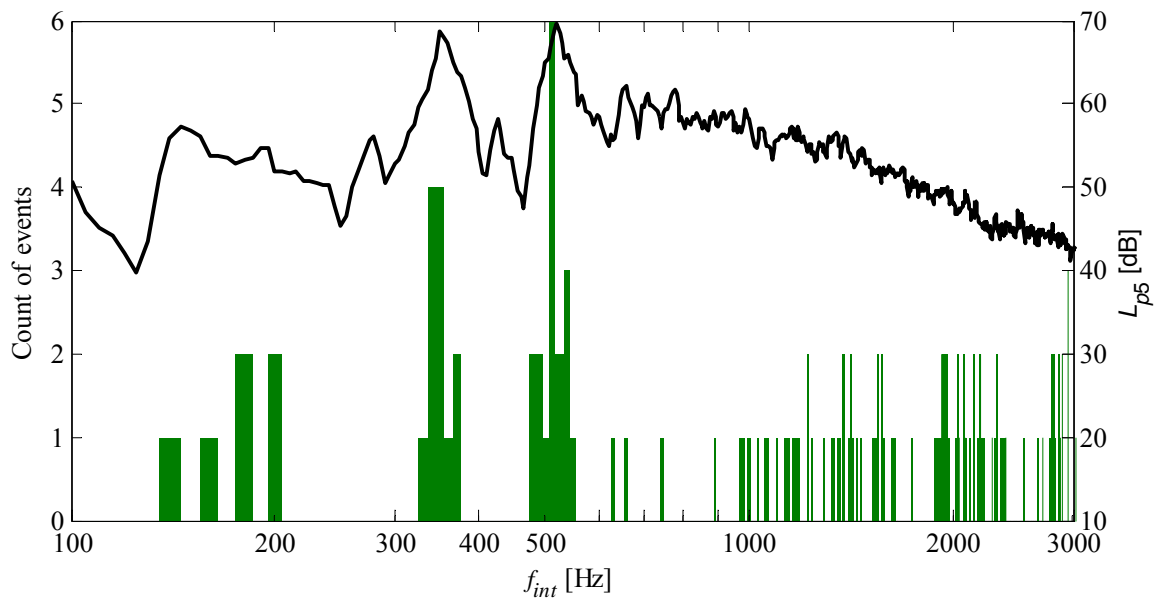

Figure 12. Resulting interaction frequency of the rotating coherent flow structures with rotor blades, compared with the free-field sound pressure level in LBM, e.g. from probe pair *R*138-*C*01-*Az*04 and -*Az*05.

Results from all probe pairs around 360°

While the analysis using a single pair of probes is by no means invalid, it presents a rather localized outlook on the modal patterns in the flow. To get a statistically significant analysis, the method shown above can be carried out for all 25 probe pairs (with $\Delta\theta = 12°$) around the full 360° of the circumference at certain spanwise (radial) and chordwise positions. For instance, at the chordwise position *C*01 and spanwise (radial) *R*138, the most important character of the detected coherent structures in terms of mode order, rotational speed and the interaction frequency are shown in Figure 13 and 14. The latter represent the statistical distribution of the identified modes over a full 360° of evaluation and thus gives a description of the modes found along the circumference for this particular position.

For the interaction frequency chart in Figure 14 especially, it can be seen that the coherent structures identified seem to greatly contribute at the location of narrowband humps whose production mechanism seems to take root in the tip clearance flow.

C. Spatial Distribution of Detected Rotating Coherent Flow Structures

Using all the probes available in the blade passages as depicted in Figure 6, a complete overview of the coherent flow structures and their interactions with the blades in the tip region can be presented. The analysis was carried out across all available spanwise positions (*R*110 to *R*146) and along 10 chordwise positions (*C*01 to *C*10) from the leading edge to the trailing edge. However, the modal analysis showed that results under the spanwise position of *R*130mm had such a weak coherence that it made the analysis impossible, indicating that few coherent structures could be detected in the flow at these positions. The results for the remaining 50 positions were coalesced to provide

a comprehensive analysis of the distribution of the coherent structures detected using the modal method, and the contribution of each spatial position is marked by the color of the monitoring points in Figure 15.
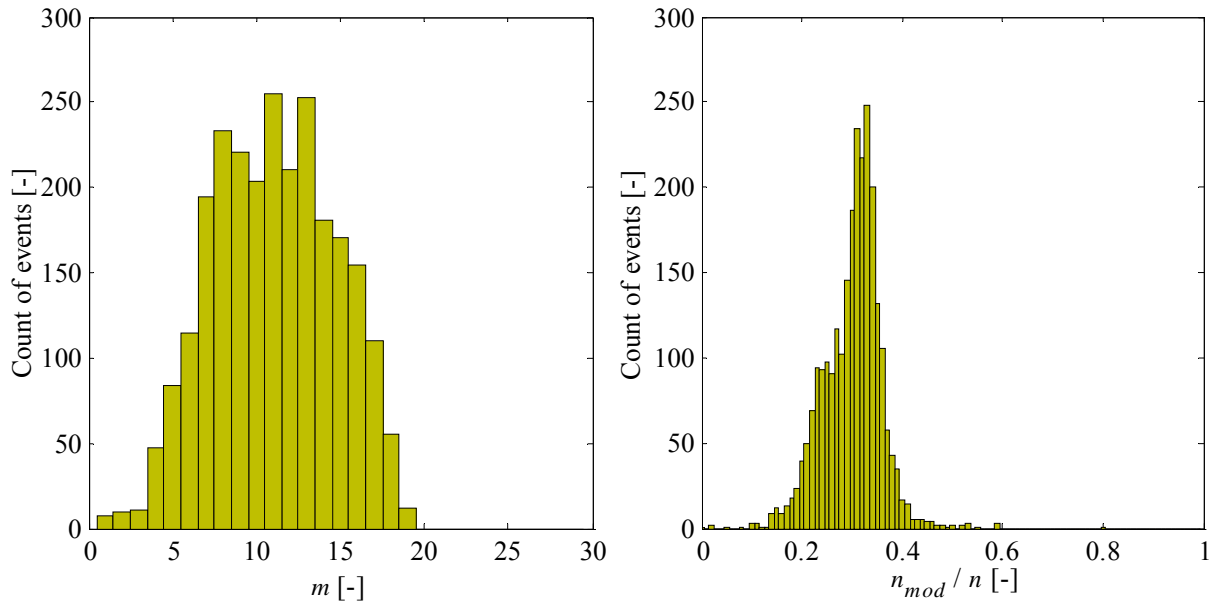

Figure 13. The mode order (left) and corresponding rotational speed (right) of the detected coherent flow structures, resulted from all probe pairs around 360°, e.g. at position R138-C01 around 360°.
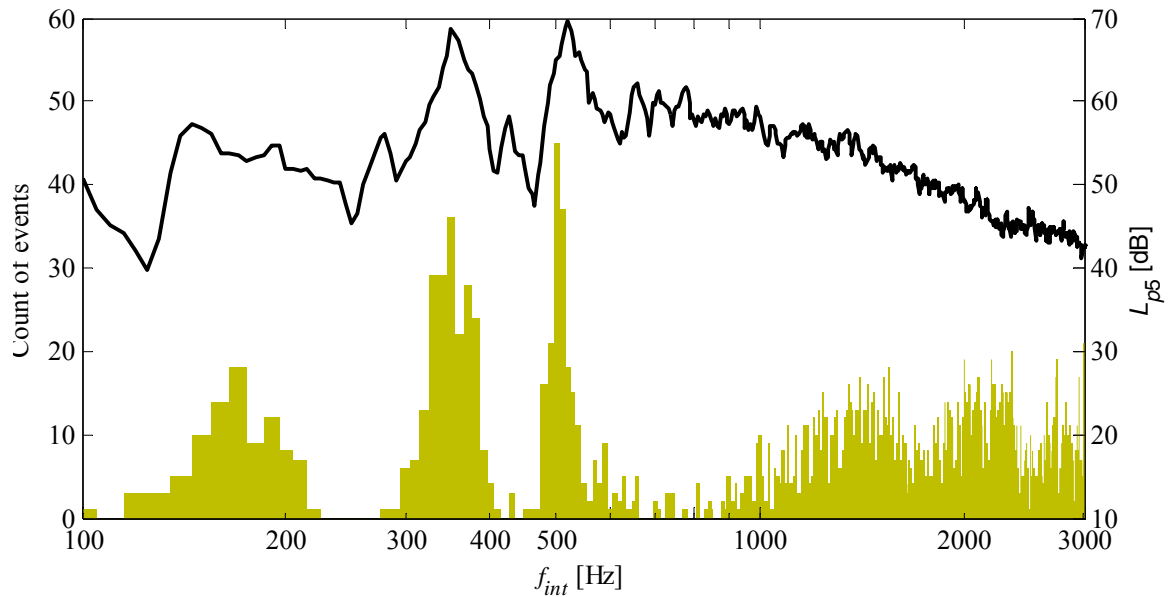

Figure 14. Resulting interaction frequencies of the rotating coherent flow structures with rotor blades, compared with the free-field sound pressure level in LBM, e.g. at position R138-C01 around 360°.
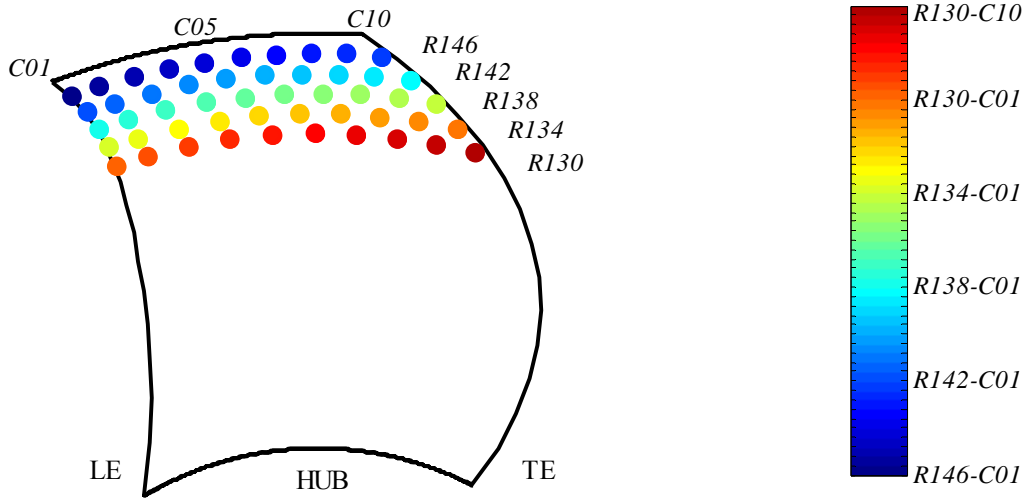
Figure 15. Color map for the chord- and spanwise distribution of monitoring points, used in Figure 16

The results are presented in Figure 16, according to the event frequency of occurrence of the detected coherent structures captured from different positions, in terms of the mode order, rotational speed and the interaction frequency. Some interesting points are worth mentioning:

- All three humps observed in the predicted sound power spectrum can be perfectly rebuilt; not only the frequencies but also the shape of the hump match very well. Even the relative levels of the humps is reproduced quite well.
- The most coherent flow structures are observed in the vicinity of the blade tip (R146-R142) and concentrated in the leading edge region of the blades (C01-C05), which is another strong hint at the tip vortices interaction.

As a conclusion, the correlation analysis of the LBM flow field data clearly shows that the narrowband humps related to tip clearance noise are generated from an interaction of the impeller blades with coherent flow structures being present in the tip region and the leading edge region of the blades. The coherent flow structures can be understood as a mixture of circumferential modes of different mode orders. The most relevant are multiples of the impeller blade number, here m = 5, 10, and 15. For this particular configuration, they rotate at approximately 30% of the impeller speed in the same direction as the impeller. The rotational speed of the different modes scatters slightly which results in humps rather than sharp peaks in the acoustic far field spectrum.

An interesting question is, how are the relatively abstract descriptors "coherent flow structure" and "mode" linked to the more intuitively characterized the tip clearance flow. In order to answer that question, the LBM flow field data can be visualized applying filtering techniques. This will be presented in the following section.

D. Visualisation of Detected Rotating Coherent Flow Structures

In Figure 17 a) the tip clearance vortex is illustrated with iso-surfaces of λ_2-criterion[32], colored according to the rotational speed as seen in the rotational frame of reference ($1-n_{mod}/n$). The range of the color map for the rotational speed is set to $0.5 < (1-n_{mod}/n) < 0.9$, which corresponds to $0.1 < n_{mod}/n < 0.5$ in Figure 16. Consequently, the vortex structures, which do not rotate or rotate almost as fast as the impeller, are denoted in blue. Note that this figure only depicts the flow field in an annular region around the blade tips containing the upper half of the blade cascade. In the next step, they are filtered out, which yields Figure 17 b). These remaining structures are the slowly rotating coherent flow structures detected from the correlation analysis.

As a conclusion, processing and visualizing the high resolution LBM flow field data reveals that the slowly rotating coherent flow structures or modes as detected by the previous correlating analysis are indeed part of the unsteady tip clearance vortex structures. They are hidden in a complex spatially and temporally inhomogeneous flow field, but can be recovered by means of appropriate filtering techniques.
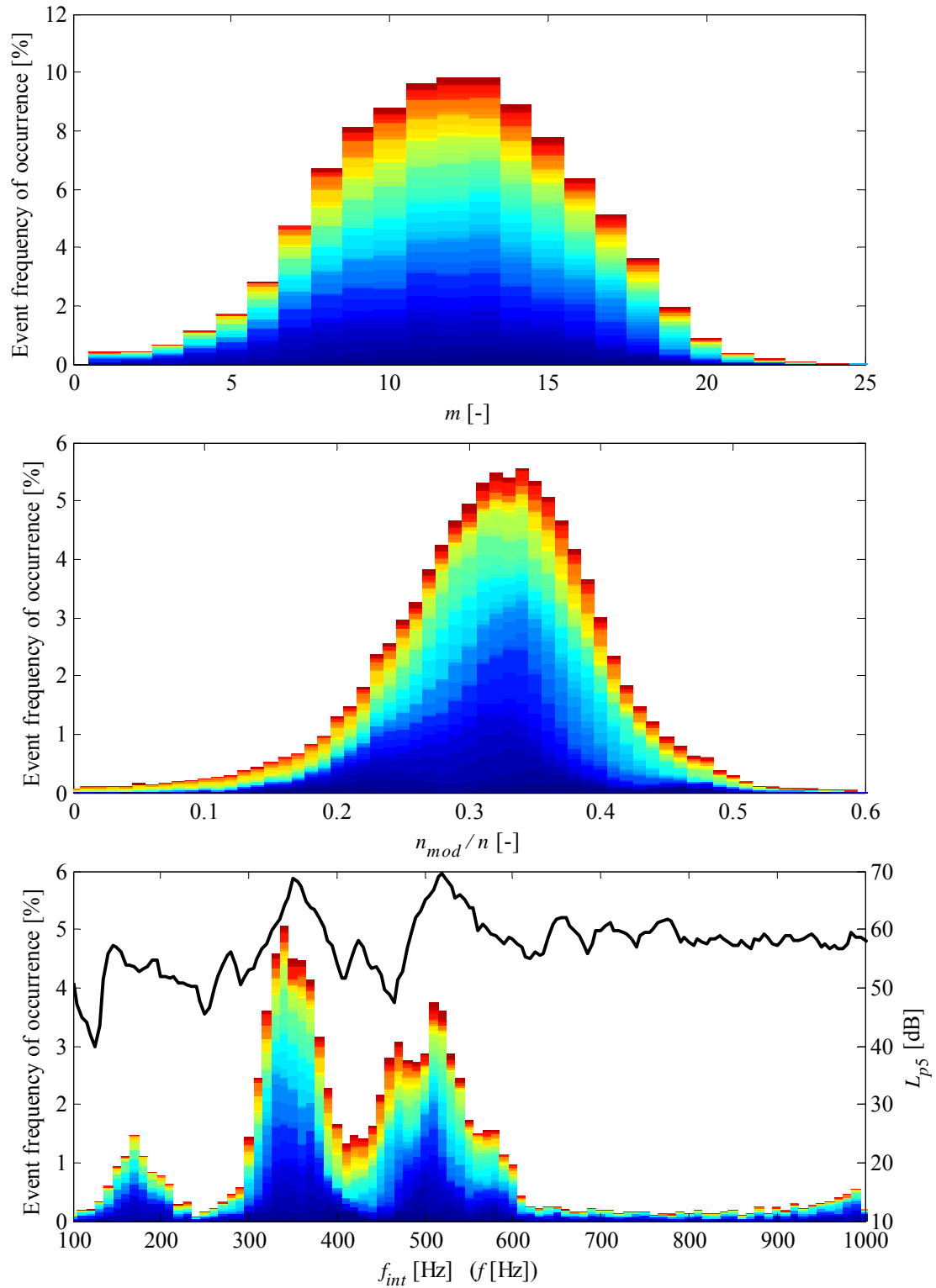
Figure 16. Spatial distribution of coherent flow structures in varying chordwise and spanwise positions detected over all blade passages in the rotational frame from the LBM results.
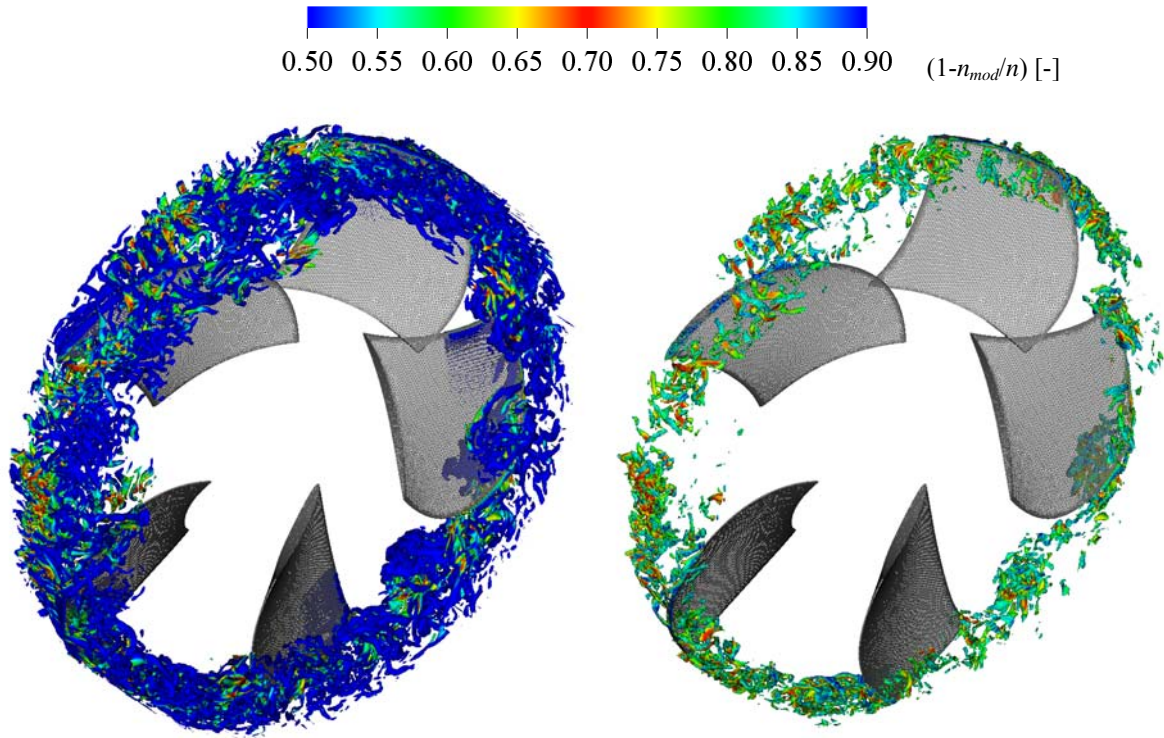
Figure 17. Left: Superimposed tip clearance vortex visualized with isosurfaces of λ_2-criterion with value of -200 1/s^2, colored with normalized rotating speed considered in the rotational reference frame (1-n_{mod}/n); right: filtered tip clearance vortex from a) with threshold of $0.6 < (1-n_{mod}/n) < 0.8$.

IV.   Conclusions and Outlooks

The present paper has focused on the identification of the mechanisms responsible for the generation of narrowband tip clearance noise in the free-field in low-speed axial fans. To that end, a full-scale experimental apparatus was represented using LBM simulations to study the flow features of a typical axial fan at varying tip clearances. It was shown that the simulations accurately reproduced the global aerodynamic and aeroacoustic characteristics of the experiment for the selected operating points, with the increased tip clearance leading to increases in broadband noise produced as well as the appearance of narrowband humps. Some near-field aerodynamic features were also well represented by the LBM simulations for the larger tip clearance which were associated in previous publications with the generation of narrowband tip clearance noise in axial fans[3].

Working under the assumption that coherent structures generated from the tip gap flow and their interaction with the blades are responsible for the narrowband humps observed in the acoustic spectra, a modal analysis method based on work carried out at Penn State University[24-27] and the University of Siegen[28, 29] was used in a novel fashion to identify the modal patterns generated and their interaction with the blades. The correlation analysis of the LBM flow field data clearly shows, that the narrowband humps are related to tip clearance noise that is generated by an interaction of coherent flow structures being present in the tip region near the leading edge of the impeller blades. The coherent flow structure can be understood as a mixture of circumferential pressure modes of varying mode orders. The most relevant ones are multiples of the impeller blade number. They rotate with approximately 30% of the impeller speed, in the same direction as the impeller. The rotational speed of the different modes is slightly scattered which results in humps rather than sharp peaks in the acoustic far field spectrum. The visualization of the identified structures shows that they are indeed parts of the unsteady tip clearance vortex structures. They are hidden in a complex spatially and temporally inhomogeneous flow field, but can be recovered by means of appropriate filtering techniques.

References

[1]Zhu, T., and Carolus, T. H. "Experimental And Unsteady Numerical Investigation of the Tip Clearance Noise of an Axial Fan," *ASME 2013 Turbine Blade Tip Symposium*. Hamburg, Germany, 2013, p. V001T04A001.

[2]Zhu, T., and Carolus, T. "Experimental and Numerical Investigation of Tip Clearance Noise of an Axial Fan Using a Lattice Boltzmann Method," *Fan 2015*. Lyon, France, 2015.

[3]Kameier, F., and Neise, W. "Rotating Blade Flow Instability as a Source of Noise in Axial Turbomachines," *Journal of Sound and Vibration* Vol. 203, 1997, pp. 833-853.

[4]März, J., Hah, C., and Neise, W. "An Experimental and Numerical Investigation Into the Mechanisms of Rotating Instability," *Journal of Turbomachinery* Vol. 124, 2002, pp. 367-375.

[5]Pardowitz, B., Tapken, U., Sorge, R., Thamsen, P. U., and Enghardt, L. "Rotating Instability in an Annular Cascade: Detailed Analysis of the Instationary Flow Phenomena," *Journal of Turbomachinery* Vol. 136, 2014.

[6]Pardowitz, B., Tapken, U., Neuhaus, L., and Enghardt, L. "Experiments on an Axial Fan Stage: Time-Resolved Analysis of Rotating Instability Modes," *Journal of Engineering for Gas Turbines and Power* Vol. 137, No. 6, 2015.

[7]Magne, S., Moreau, S., and Berry, A. "Subharmonic Tonal Noise from Backflow Vortices Radiated by a Low-Speed Ring Fan in Uniform Inlet Flow," *The Journal of the Acoustical Society of America* Vol. 137, 2015, pp. 228-237.

[8]Moreau, S., and Sanjosé, M. "Sub-Harmonic Broadband Humps and Tip Noise in Low-Speed Ring Fans," *The Journal of Acoustical Society of America* Vol. 139, No. 1, 2016, pp. 118-127. doi: 10.1121/1.4939493

[9]Piellard, M., Coutty, B., Le Goff, V., Vidal, V., and Pérot, F. "Direct Aeroacoustics Simulation of Automotive Engine Cooling Fan System: Effect of Upstream Geometry on Broadband Noise," *20th AIAA/CEAS Aeroacoustics Conference*. Atlanta, GA, USA, 2014.

[10]Lallier-Daniels, D., Piellard, M., Coutty, B., and Moreau, S. "Aeroacoustic Study of an Axial Ring Fan using Lattice-Boltzmann Simulations and the Ffowcs-Williams and Hawkings Analogy," *International Symposium on Transport Phenomena and Dynamics of Rotating Machinery*. Hawaii, Honolulu, 2016.

[11]Carolus, T. "Entwurfsprogramm für Niederdruck-Axialventilatoren dAX-LP." Siegen, 1987-2015.

[12]Zhu, T. "Akustische Nachberechnung von Ventilatoren - Hauptarbeitspaket C: Aeroakustisches Validierungsexperiment. FLT Nr.: L236, Final report." University of Siegen, Institute of Fluid- and Thermodynamics, Siegen, 2012.

[13]Frisch, U., Hasslacher, B., and Pomeau, Y. "Lattice-Gas Automata for the Navier-Stokes Equation," *Physical Review Letters* Vol. 56, No. 14, 1986, pp. 1505-1508.

[14]Guo, Z., Zheng, C., and Shi, B. "Discrete Lattice Effects on the Forcing Term in the Lattice Boltzmann Method," *Physical Review E* Vol. 65, No. 046308, 2002.

[15]Chen, H., Kandasamy, S., Orszag, S., Shock, R., Succi, S., and Yakhot, V. "Extended Boltzmann Kinetic Equation for Turbulent Flows," *Science* Vol. 1, No. 301, 2003, pp. 633-636. doi: 10.1126/science.1085048

[16]Chen, H., Orszag, S. A., Staroselsky, I., and Succi, S. "Expanded Analogy between Boltzmann Kinetic Theory of Fluid and Turbulence," *Journal of Fluid Mechanics* Vol. 519, 2004, pp. 301-314. doi: 10.1017/S0022112004001211

[17]Chen, H. "Volumetric Formulation of the Lattice Boltzmann Method for Fluid Dynamics: Basic Concept," *Physical Review E* Vol. 58, No. 3, 1998, pp. 3955-3963.

[18]Pérot, F., Kim, M.-S., Moreau, S., Henner, M., and Neal, D. "Direct Aeroacoustics Prediction of a Low Speed Axial Fan," *16th AIAA/CEAS Aeroacoustics Conference*. 2010.

[19]Perot, F., Kim, M.-S., Meskine, M., and Freed, D. "NREL Wind Turbine Aerodynamics Validation and Noise Predictions Using a Lattice Boltzmann Method," *18th AIAA/CEAS Aeroacoustics Conference, .* Colorado Springs, 2012.

[20]Mann, A., Perot, F., Kim, M.-S., Casalino, D., and Fares, E. "Advanced Noise Control Fan Direct Aeroacoustics Predictions Using a Lattice-Boltzmann Method," *18th AIAA/CEAS Aeroacoustics Conference*. Colorado Springs, CO, 2012.

[21]Perot, F., Kim, M.-S., Goff, V. L., Carniel, X., Goth, Y., and Chassaignon, C. "Numerical Optimization of the Tonal Noise of a Backward Centrifugal Fan Using a Flow Obstruction," *Noise Control Engineering Journal* Vol. 61, No. 3, 2013, pp. 307-319.

[22]Zhang, R., Shan, X., and Chen, H. "Efficient Kinetic Method for Fluid Simulation Beyond Navier-Stokes Equation," *Physical Review E* Vol. 74, No. 046703, 2006.

[23]Brès, G., Pérot, F., and Freed, D. "Properties of the Lattice-Boltzmann Method for Acoustics," *15th AIAA/CEAS Aeroacoustics Conference (30th AIAA Aeroacoustics Conference)*. Miami, Florida, USA, 2009.

[24]Mongeau, L., Thompson, D. E., and McLaughlin, D. K. "Sound Generation by Rotating Stall in Centrifugal Turbomachines," *Journal of Sound and Vibration* Vol. 163, No. 1, 1993, pp. 1-30. doi: 10.1006/jsvi.1993.1145

[25]Bent, P. H. "Experiments on the Aerodynamic Generation of Noise in Centrifugal Turbomachinery." Vol. Ph.D., Pennsylvania State University, 1993.

[26]Bent, P. H., McLaughlin, D. K., and Thompson, D. E. "Identification of Non-Tonal Noise Sources in Centrifugal Turbomachinery," *ASME -PUBLICATIONS- FED* Vol. 168, 1993, pp. 207-216.

[27]Tetu, L. G. "Experiments on the Aeroacoustics of Centrifugal Turbomachinery." Vol. Master, The Pennsylvania State University, 1993.

[28]Wolfram, D., and Carolus, T. "Detection and Analysis of Azimuthal Modes in a Centrifugal Impeller," *The 12th International Symposium on Transport Phenomena and Dynamics of Rotating Machinery*. Honolulu, Hawaii, 2008.

[29]Sturm, M., and Carolus, T. H. "Tonal Fan Noise of An Isolated Axial Fan Rotor Due to Inhomogeneous Coherent Structures at The Intake," *Noise Control Engineering Journal* Vol. 60, No. 6, 2012, pp. 699-706.

[30]Welch, P. D. "The Use of Fast Fourier Transform for the Estimation of Power Spectra: A Method Based on Time Averaging Over Short, Modified Periodograms," *IEEE Transactions on Audio Electroacoustics* Vol. AU-15, No. 2, 1967, pp. 70-73.

[31]Sturm, M., Sanjose, M., Moreau, S., and Carolus, T. "Aeroacoustic Simulation of an Axial Fan Including the Full Test Rig by Using the Lattice Boltzmann Method," *Fan 2015*. Lyon, France, 2015.

[32]JEONG, J., and HUSSAIN, F. "On the Identification of a Vortex," *Journal of Fluid Mechanics* Vol. 285, 1995, pp. 69-94.